Measurements of Spatial Line Emission Profiles in the Main Scrape-Off Layer of the DIII-D Tokamak

M. Groth, R.M. Ellis, N.H. Brooks, M.E. Fenstermacher, C.J. Lasnier, W.H. Meyer, J.M. Moller

June 5, 2009

LAWRENCE
LIVERMORE
NATIONAL
LABORATORY

Disclaimer

This document was prepared as an account of work sponsored by an agency of the United States government. Neither the United States government nor Lawrence Livermore National Security, LLC, nor any of their employees makes any warranty, expressed or implied, or assumes any legal liability or responsibility for the accuracy, completeness, or usefulness of any information, apparatus, product, or process disclosed, or represents that its use would not infringe privately owned rights. Reference herein to any specific commercial product, process, or service by trade name, trademark, manufacturer, or otherwise does not necessarily constitute or imply its endorsement, recommendation, or favoring by the United States government or Lawrence Livermore National Security, LLC. The views and opinions of authors expressed herein do not necessarily state or reflect those of the United States government or Lawrence Livermore National Security, LLC, and shall not be used for advertising or product endorsement purposes.

Measurements of spatial line emission profiles in the main scrape-off layer of the DIII-D tokamak

M. Groth,[1] R.M. Ellis,[1] N.H. Brooks,[2] M.E. Fenstermacher,[1] C.J. Lasnier,[1]

W.H. Meyer,[1] J.M. Moller[1]

[1]*Lawrence Livermore National Laboratory, P.O. Box 808, Livermore, California*

[2]*General Atomics, P.O. Box 85608, San Diego California 92186-5608, USA*

Abstract. A video camera system is described that measures the spatial distribution of visible line emission emitted from the main scrape-off layer (SOL) of plasmas in the DIII-D tokamak. A wide-angle lens installed on an equatorial port and an in-vessel mirror which intercepts part of the lens' view provide simultaneous tangential views of the SOL on the low-field and high-field sides of the plasma's equatorial plane. Tomographic reconstruction techniques are used to calculate the 2-D poloidal profiles from the raw data, and 1-D poloidal profiles simulating chordal views of other optical diagnostics from the 2-D profiles. The 2-D profiles can be compared with SOL plasma simulations; the 1-D profiles with measurements from spectroscopic diagnostics. Sample results are presented which elucidate carbon transport in plasmas with toroidally uniform injection of methane and argon transport in disruption mitigation experiments with massive gas jet injection.

I. INTRODUCTION

Understanding particle transport in the scrape-off layer (SOL) of existing tokamaks is important for controlling particle and heat exhaust and migration of eroded wall materials in future tokamaks, such as ITER [1]. Radiation in the SOL is one of the main plasma parameters that determines the intensity of plasma-wall interaction at the divertor target plates. Measurements of the spectral line emission and its spatial intensity distribution are needed to experimentally assess the locations of hydrogen recycling and impurity sources, and to locate the regions of volumetric power losses. They are also needed to validate analytic and numerical SOL models that predict the SOL performance in existing and future fusion devices. Also, impurity flows in the SOL govern the distribution of hydrogen co-deposition associated with impurities sputtered from the plasma-facing walls [2]. Measurements of the impurity emission profiles provide key data to elucidate the impurity flow pattern in the main SOL.

Imaging with video cameras is a non-intrusive technique of measuring the toroidal and poloidal intensity distribution of line radiation in the visible wavelength range [3–9]. The advantage of an imaging system over discrete line-of-sight monitors lies in the greater spatial wealth of the measurements. For nearly toroidally symmetric plasmas, like tokamaks, tangentially viewing imaging systems can be employed to obtain the poloidal intensity distribution profiles after tomographic reconstruction of the raw image data. Charge injection device (CID) cameras with tangential viewing geometries have been used in the DIII-D tokamak [10] to yield two-dimensional emission profiles of deuterium and carbon in the divertor region, in both the visible [3] and ultraviolet [11]). In comparison to charge coupled device (CCD) cameras, CID images are less susceptible to

neutron damage and thus more suitable for measurements in the DIII-D radiation environment. Several years ago, an equatorial camera system with a tangential view was installed on DIII-D to enable measurements of the high-field side (HFS) SOL; recent improvements to that system have enabled simultaneous measurements of the low-field side (LFS) SOL. This article describes the hardware, diagnostic setup, calibration, and experimental results of the midplane camera system built as part of the Lawrence Livermore National Laboratory (LLNL) research collaboration at the DIII-D National Fusion Facility.

II. DESCRIPTION OF LLNL MIDPLANE CAMERA HARDWARE

A. Camera field-of-view

A midplane tangential view of the HFS SOL, and plasma-wall interaction on the LFS of the DIII-D tokamak, was obtained by installing a camera with a wide-angle collection lens outside the tangential viewport at 120°, looking in the counter clockwise direction (Fig. 1). Since the port geometry precluded a tangential view of the LFS SOL region, a stainless steel (SS-316) mirror was installed, at a later time, inside the vacuum vessel of the same port to sample the emission from the SOL in the clockwise toroidal direction (see Section III.C). The primary field-of-view of the system toroidally spans about 90° of the vacuum chamber in the counter-clockwise direction (Fig. 2) and is vertically centered about the midplane of the vessel. The full vertical extent of the primary view on the HFS is ~1 m, including the HFS wall; and ~2 m on the far LFS wall. Along the LFS equatorial plane the view includes the ion cyclotron radio frequency antenna at 0°, the neutral beam port at 30°, and several smaller diagnostic ports at 45° and 60°. A direct view the LFS

bumper limiter at 95° (one of three distributed roughly equally in toroidal angle) is obscured by the port edge. To avoid reflected light from contaminating measurements in the mirror's view, the dimensions of the mirror (5 cm wide × 10 cm tall) were designed to match the size of a view dump installed on the side wall of the midplane port at 150°. The mirror gives a 10 × 30 cm view area of the SOL at the plane of tangency. This viewing geometry enables emission measurements in the LFS SOL for DIII-D plasmas with gaps between the separatrix and outer wall in the range of 8 to 12 cm.

B. Optical relay system in the tokamak hall

A collection lens (Schott IG-1635, [12]) installed at the viewport images the light from the plasma onto the front part of a coherent image guide that relays the light from the port to the camera system (Fig. 3). Limited space at the viewport and the necessity to place the camera in a magnetic field < 0.02 T required the installation of the camera on a platform about 1.5 m back from the toroidal field coils. The two-piece, plano-convex collection lens and the front end of the image guide are clamped inside a Delrin® (Dupont™) block and mounted in front of the viewport on a stainless steel (SS-316) platform. The short focal length lens (6 mm) in combination with the 4 mm square image guide gives rise to a view cone angle of 40°. The fiber image guide (Schott IG-154) is a square array of 400 × 400 individual fibers of 10 μm diameter made of commercial glass (silicone oxide with trace levels of potassium, sodium, and aluminum). The image guide's numerical aperture (NA) is 0.56 (f/0.9), providing efficient coupling of the light imaged on it by the f/1.1 collection lens. The manufacturer specifies a nominal transmissivity of 35% at 550 nm for the 2.74 m-long image guide. Since its light transmission significantly decreases with exposure to ionizing radiation during DIII-D

operations, monitoring of the transmission was performed routinely to maintain the absolute calibration of the system (see Section III.B).

The image relayed to the distal end of the image guide is collimated by a telescope lens (Computar 25 mm lens, f/1.3), with its focus set to infinity, spectrally filtered for wavelengths of interest using narrow-bandpass interference filters, and refocused with a magnification of two on the CID sensor (Fig. 4). Neutral density filters [optical density (OD) 0.3–1.5] are used to attenuate the image brightness to prevent saturation of the CID sensor for its available settings of exposure time and gain. The interference and neutral density filters (diameter 25 mm) are installed in a dual-wheel filter-changer (Suagaro Scientific Corporation, five slots for each group of filters), which is remotely controllable from outside the tokamak hall. A list of interference filters is given in Table 1.

To accommodate the anticipated intensity difference between the HFS and LFS views, a custom-made neutral density filter is inserted into the HFS view area at the distal end of the image guide. Partial attenuation of the HFS image relative to the LFS was achieved with a thin-film Wratten filter (Kodak) with an L-shaped cutout corresponding to the mirror view (Fig. 4). The filter is mounted on a X-Y translation stage with a fine-threaded micrometer that permits adjustment of the filter location with respect to the distal end of the image guide.

A second telescope lens (Fujinon 50 mm lens, f/1.4), focus set to infinity focuses the filtered light onto the CID sensor. The resulting image fills about 75% of the sensor's active area.

C. Description of gated, image-intensified camera

The camera is a custom-made product of Xybion Electronic Systems consisting of an image intensifier (Delft Electronic Products), a glass taper, and a standard CID imager (Thermo Fisher, CIDTEK 3710D) [13]. The GEN II intensifier functions as a fast shutter, photon-to-current converter, and amplifier. Its multi-alkali photo-cathode has a spectral response spanning the range of 400 to 800 nm. The intensifier's microchannel plate allows integration times between 300 ns and 33 ms, with rise times of the order 1 ns. Signal amplification of up to four orders of magnitude can be achieved with the present unit. The gain in photon current closely follows a power-law with respect to the setting on the control unit. The electrons emitted from the photo-cathode carry energies of several kilo electron volts. As they penetrate the aluminum-overcoated phosphor screen, they are converted into photons with a high gain factor. The phosphor screen used in this application (Proxitronic, type P20) has a characteristic spectral-energy distribution peaking around 500 nm and a persistence time scale $< 100 \, \mu$s. The system can be triggered internally on each vertical sync pulse of the CID sensor readout or externally using a TTL-pulse based triggering unit. The glass taper demagnifies the image formed on the phosphor screen onto the 9×7 mm (width $\times$ height) active area of the CID sensor. The sensor's active area includes 754×484 displayed pixels. The dynamic range of the CID sensor is 8 bits, providing adequate contrast within the image for an intensity range of two orders of magnitude. The unit outputs a 2:1 interlaced video signal (RS-170, North America NTSC format) with an integration time for odd or even fields alone of 16.7 ms. Operating the intensifier in internal triggering mode, and limiting the gate times

to less than 16.7 ms, the intensifier places just one gate pulse in each even video field and none in the odd fields.

D. Data acquisition system

The intensifier gating signal and CID video signal are transferred between the DIII-D tokamak hall and the control unit outside the hall via ~30 m long cables. The maximum cable length for undistorted signal and video transmission was determined in dedicated off-site tests prior to the camera installation on DIII-D. The video signal, and the video gate and field times are relayed another 100 m from the camera control unit to the DIII-D control room via an optical link (American Fibertek). The data are recorded, processed, and stored to random access memory (RAM) on a PC using a video frame grabber [National Instruments (NI) PCI-1407] and counter/timer (NI PCI-6602). The acquisition software is based on NI's LabVIEW. After the plasma discharge, the processed data are transferred to an MDSplus data server. During a 5-s DIII-D discharge, approximately 45 MB of video data are acquired. LabVIEW-based software also handles the subsequent image and timing processing, and visualization of the data after the plasma discharge.

III. CALIBRATION OF THE CAMERA SYSTEM

A. In-situ calibration procedures

In-situ calibration of the entire camera system, including all optical components, amplifiers, transmitters and receivers, and the data acquisition system, are performed annually when the tokamak vacuum vessel is vented to air and accessible for manned entry. The calibration procedure yields the sensitivity of the complete chain of optical and electronic components, including the image guide. Because of its susceptibility to transmission loss due to ionizing radiation produced during plasma operations, the image is routinely recalibrated on a test bench (see Section III.B). The main and mirror views are spatially calibrated using cardboard placards with reflective markers at known radial and vertical locations [Fig. 5(a)]. Images of the placards inside the vessel are typically recorded at three different toroidal locations within the depth-of-field of the camera system. The images are used as input to the 3-D rendering code POVRAY [14] to generate a virtual camera with the same field-of-view [Fig. 5(b)]. To convert the measured count rates at the video frame grabber into photon flux, a light source (Integrating Sphere 454 series, Optronic Laboratories [15]) is installed in the DIII-D vacuum vessel during the vent. Since the output area of the light source (~100 cm^3, circular cross-section) is considerably smaller than the camera field-of-view (~1 m^3 at the plane of tangency), recordings of the light source are made at different radial and vertical locations. For each interference filter, images of the light source output are taken at different gate times and gain, covering the range of settings used during tokamak operations. The neutral density filters are calibrated for their actual light attenuation.

Camera background images are taken for each setting of the camera intensifier. The image data is processed for count rates at given lamp luminosity and transferred to a calibration file on the DIII-D main computer system. Over a period of four years, or approximately 10 hours of plasma operations, no systematic degradation of the camera system — apart from the image guide as previously mentioned — was observed (Fig. 6), indicating that the lenses, filters, and CID sensor did not suffer significantly from ionizing radiation. Over the same period, the background signal ("black level") of the CID sensor increased from 1 count to 5 counts averaged across the active pixel area.

B. Calibration of light transmission loss by the image guide

The spectral transmission of visible light in the wavelength range 350–800 nm by the Schott image guide IG-154 was routinely monitored because glass optical fibers, in general, suffer from degradation of transmission when exposed to ionizing radiation. The neutron and γ-radiation produced in today's fusion experiments is sufficient to significantly reduce the transmission in optical fibers on both short-term and long-term time scales [16,17]. The choice of the IG-154 as the image guide in this application was dictated by the required, large field-of-view at sufficiently high spatial resolution (1–2 cm), and the limited availability of high-grade fused silica image guides. Previous studies of the IG-154 in another camera system on DIII-D showed significant, long-term reductions (factor of 10, or more) in the transmission over the course of 750 to 1500 s of integrated deuterium-deuterium operation [3]. In this study, a dedicated effort was made to monitor the transmission in the spectral range from 350 to 800 nm. Production of radiation-induced photons in the optical fiber (scintillation) as described in [16, 17] could

not be investigated with the present equipment, as these photons cannot be discriminated against neutron-induced speckles on the CID sensor.

The spectral throughput of the IG-154 was measured using a calibrated light source (Unisource 600, output range 400–800 nm) and an Ocean Optics USB 2000 spectrometer. To avoid changing the focus of the front and distal lenses used during plasma operation, the entire optical collection and transmission assembly was mounted between the light source and the spectrometer. An f/2.0 miniature lens imaged the light from the distal end of the image guide into the spectrometer. The light source output and spectrometer background data were recorded along with the spectrum of the transmitted light on a personal computer connected to the spectrometer via Universal Serial Bus (USB). Typically, each transmission spectrum was integrated over 1 s using the software provided by Ocean Optics.

The strongest degradation of the visible transmission was measured in the spectral interval 450–500 nm, where a reduction of up to a factor of 5 was observed [Figs. 7(c) and 8]. The transmission loss in the 600–650 nm range is significantly smaller — only a factor of 1.5. The transmission of an unexposed fiber bundle is consistent with data provided by Schott [12]. The transmission degradation increased with neutron and γ ray exposure, and no saturation of the signal loss was observed for the four sample bundles shown in Fig. 8. At a neutron fluence of 10^{16} n/m^2 the total attenuation at 450 nm is of the order 6 dB/m, resulting in a transmission loss only 2% of that of an unexposed image guide. At this point of transmission degradation, the IG-154 was replaced. The transmission loss among the exposed image guides was remarkably consistent over the

neutron fluence explored, despite the fact that the image guides were drawn from different batches during manufacturing.

The neutron fluence was calculated based on the measured neutron rates in DIII-D [18], accumulated over the period during which the image guide was exposed, and assuming a neutron point source at a distance of 3 m to the image guide. Translating the initial 2.45 MeV neutron flux into an absorbed dose at the image guide location requires sophisticated neutronics calculations, which have not been performed as part of this study. Most of the radiation-induced losses are caused by γ radiation from inelastic scattering of neutrons and (n,γ) capture reactions in the neutron moderation process [19]. Previous neutronics calculations for DIII-D [20] indicated a broad energy spectrum of γ rays in the range of several electron volts to 10 MeV. The estimated ionization dose (Si equivalent) for 1 MeV neutrons and fluence of 10^{16} n/m^2 is of the order 100 rad to 1 krad [21].

The transmission of an exposed image guide was recovered to nearly its initial value by heating the IG-154 in a vacuum furnace at 150°C for 48 h [Fig. 7(c)], without loss of image integrity [Fig. 7(a) versus Fig. 7(b)]. For a single image guide the transmission was measured prior to installation on DIII-D, after exposure to DIII-D neutron fluence of 6×10^{16} n/m^2 prior to the bake in an off-site vacuum furnace, and after the bake. In the wavelength range around 650 nm the transmission recovered from 60% to nearly 100% of the initial transmission, while in the range around 500 nm the recovery was from 40% to about 90%. The dependence of the transmission loss with neutron exposure for the refurbished image guide will be studied in the DIII-D 2009 experimental campaign. To

mitigate the transmission loss during tokamak operation, maintaining an image guide temperature of 150°C may be implemented in future campaigns.

C. Assembly and calibration of the in-vessel mirror

Using the existing ex-vessel collection optics, a 2-D view of the LFS SOL at the midplane was achieved by installing a mirror inside the tokamak primary vacuum (Section II.A). The mirror is made of non-magnetic stainless-steel (SS-316), with the front surface polished to a flatness of $\lambda/2$ at 650 nm. It is mounted against the shutter chassis of the beam emission spectroscopy (BES) system. To align the view with respect to the vacuum vessel, the mount permits the mirror to be shifted radially as well as vertically, and to be rotated along its vertical axis. After the final alignment, the mount is locked down with set screws and tack-welded. The mirror view is terminated by a view dump attached to the sidewall of the 150° midplane port (Fig. 1). The dump is made of stainless steel (SS-316) with V-shaped vertical grooves of half-width 2.2 mm and vertex angle of 30°. It has a black chromium finish to further reduce specularly reflected light.

Calibration of the spatial extent of the view and of the mirror reflectivity was performed with the same equipment used for the primary view (Section III.A). The aperture size of the integrating sphere light source subtends a cone whose elliptical intersection with the mirror covers nearly two-thirds of the mirror's horizontal extent and about one-fourth of its vertical extent. The initial mirror reflectivity at 656 nm was ~75% (Fig. 9). Inspection of the mirror surface after plasma operation in 2006 (~ 2 h of plasma operations) showed rainbow-like discoloration at the top end of the mirror and an oblique black stripe extending from the left top to the center bottom (Fig. 10). The shape of the discoloration suggests deposition of material in the plasma-shadowed region of the port.

Post-operation calibration showed a two to three-fold decrease of the mirror reflectivity at two test wavelengths due to deposits on the mirror surface (Fig. 9). The reflectivity did not vary along the vertical extent of mirror surface. Ex-situ analysis of the reflectivity and the composition of deposits is in progress and will be reported separately.

IV. ANALYSIS AND SAMPLE RESULTS

A. Tomographic inversion analyses

The pixel data at the CID sensor represents a 2-D array of emission measurements integrated along diverging tangential lines-of-sight in the tokamak chamber. Tomographic reconstruction software developed for the divertor tangential cameras [3] was adapted for the midplane view to produce 2-D poloidal profiles from the measured image data. Around the midplane, where the viewing geometry is nearly horizontal, less time-consuming techniques than tomographic reconstruction, such as Abel inversion can also be applied to calculate the 2-D poloidal profile. The geometrical line integrals are determined from the virtual camera generated from the spatial calibration data (Section III.A), and are folded into a transformation matrix, M. Assuming toroidal symmetry of the 3-D emission, the 2-D intensity distribution in the poloidal plane is obtained numerically by solving the matrix equation $AM = B$. Here, A is the 2-D poloidal profile and B is the measured pixel data. Corrections for reflections have not been included as part of this work.

To keep the transformation matrix to a manageable size and the linear regression calculations within a few CPU hours, the solution grid for the primary view is partitioned into a high-resolution region near the HFS wall (18 × 75 cells of width 2 cm and height

2 cm) and a low-resolution region elsewhere (11 × 25 cells of 12 × 6 cm). This simplification is enabled by the fact that the strongest emission comes from the HFS SOL region. The mirror view is calculated independently from the main view using an Abel inversion technique. The raw data are sampled by the video frame grabber for 640 × 240 pixels. Since the image does not fill the entire active area of the CID sensor, it is clipped by software reducing the pixel array dimensions to 310 × 120 pixels. In calculating the matrix elements (= geometrical line integrals), which is either done analytically or using a Monte-Carlo technique, only the non-zero elements are stored. The resulting transformation matrix is sparse and of the order of 10 MB, representing a tractable problem for linear regression algorithms on present-day computer systems.

The most reliable algorithm to perform the least-square regression was obtained with the routine WNNLS of the SLATEC Common Mathematical Library [22]. The algorithm allows the solution to be constrained to non-negative values. Running an inversion problem on a single-processor, 32-bit LINUX computer system takes about 30 minutes of CPU time. Several other least-square regression algorithms have also been tested, including SPARSE [23] and TSNNLS [24]. The SPARSE algorithm is significantly faster than WNNLS, however, it allows for negative solutions, which are unphysical in this application. The TSNNLS routine is also significantly faster than WNNLS and constrains the solution to non-negative values but, as found out empirically, it produces more reconstruction artifacts in the solutions than WNNLS.

Translational and rotational shifts of the camera view during plasma operations relative to the view obtained during the in-vessel calibrations require that the data images be re-aligned prior to tomographic reconstruction. These view shifts are caused primarily

by repeated removal and reinstallation of the image guide and collection lens. The same alignment software developed for the divertor cameras [3] is also used for the midplane camera. Images containing the main wall features obtained during plasma ramp down are commonly used as fiducials.

The processed data, including the calibrated and aligned 3-D image data and the 2-D poloidal profiles are stored in an MDSplus server for user-friendly data retrieval. In addition, 1-D poloidal profiles that replicate the viewing geometry of the DIII-D filterscope system [25] are also generated and stored in MDSplus. The transformation matrices, whose elements are the geometrical line integrals in the poloidal plane, are calculated in similar fashion as the 3-D integrals using POVRAY. The angular resolution is set to match the grid size of the 2-D poloidal profiles, e.g., ~1°, yielding high-resolution poloidal profiles which contain significantly more spatial detail than those achieved with the single-channel filterscope viewing the main chamber radially. The vertex point of the view chords is determined by the lens location of the filterscope. The processed profiles are compared to the measured profiles from the filterscopes, and often used to cross-calibrate the camera emission analysis.

B. Sample results

Measurements with the midplane camera system have been extensively used to elucidate poloidal particle transport in the HFS main SOL from impurity sources outside the midplane field-of-view, such as the inner divertor target plate [26]. Figure 11 shows measurements of the 3-D (a) and 2-D poloidal (b) emission profiles from doubly charged carbon ions (CIII) at 465 nm. The input data was averaged over 200 ms prior to the tomographic reconstruction to improve the signal-to-noise ratio. Using the lens location

of the single-channel radial view of the actual filterscope system as the vertex of a 100-channel virtual fan array [Fig 11(b)], the 1-D poloidal, line-integrated emission profile (as a function of vertical height, Z, along the HFS wall) is calculated [Fig. 11(c)]. The emission of the virtual camera channel at $Z = 0.2$ m is approximately a factor of 2 lower than the filterscope measurement. This discrepancy may be due to the fact that the virtual camera takes no account of the CIII emission from the LFS SOL region. However, independent measurement of the LFS CIII emission with the in-vessel mirror and tangential filterscopes show that the radial profile is dominated by emission from the HFS SOL. Since the filterscope measurement requires significantly less sophisticated analysis, the camera emission profiles may be scaled to the filterscopes.

Simultaneous measurements of the CIII emission in the HFS and LFS SOL regions around the midplane during methane injection indicate that the flow of the injected carbon is toward the HFS divertor rather than to the LFS divertor. Figure 12 shows the 3-D profiles of CIII emission from the HFS wall and the mirror views prior to (a) and during (b) the methane injection. The emission from the HFS SOL region was attenuated by a neutral density filter of OD = 1.0. Methane was injected at ~1 Pa m^3/s into the top of the plasma in toroidally symmetric fashion via the upper outer pumping plenum. The radial profiles taken at $Z = 0.5$ m in the HFS SOL, and $Z = 0$ in the LFS SOL (from the mirror) are shown in Fig. 12(c) and 12(d), respectively. During the methane injection the CIII emission from the HFS SOL increased fivefold, while that from the LFS increased only 10%. The camera measurements show that the intensity ratio between the HFS and LFS SOL is of the order 10 for these low-density, low-confinement plasmas. They are

consistent with filterscope measurements radially across the plasma and tangentially across the LFS SOL region.

Imaging with the midplane camera system during disruption mitigation experiments employing massive gas injection into the DIII-D tokamak showed that the radial motion of the neutral gas jet was arrested in the pedestal bounding the core region [27]. Figure 13 shows the 3-D profile of the emission from single ionized argon (ArII at 612 nm) taken 40 μs after the injection trigger at an integration time of 20 μs. Synchronous with the injection trigger, a localized interaction of the jet with plasma surface is visible, and the ArII emission has spread out along the magnetic field lines without indication of penetration inside the separatrix. To obtain a view of the gas leaving the injection port, the collection lens assembly was mounted 15 cm below the standard configuration. The intensifier was triggered externally on a signal from the massive gas injection system. By shifting the trigger with respect to the gas injection valve timing, a series of images during the gas injection was obtained, which elucidated the gas jet dynamics.

V. SUMMARY

New insights into the physics processes obtained in the plasma edge of tokamaks were gained by measuring the visible emission profiles in the main chamber of the DIII-D tokamak with a tangentially viewing video camera. The system provides simultaneous views on the equatorial plane of the scrape-off layer at both the high-field and low-field sides of the plasma. The midplane system complements the suite of video cameras in the upper and lower divertor maintained and operated by Lawrence Livermore National Laboratory as part of its research collaboration on the DIII-D device. The optical train includes a wide-angle lens installed behind a tangential viewport at the

midplane and a coherent fiber image guide that relays the images to an intensified, charge injection device (CID) camera. The image intensifier enables microsecond short snapshots to be taken at gains up to 10^4. An in-vessel mirror and spatially notched attenuator in the image plane permit simultaneous measurement of the emissions in the HFS and LFS SOL regions with an 8-bit CID sensor. Narrow-bandpass interference filters are used to isolate the spectral line emission from specific plasma species. An in situ calibration is performed annually to check the spatial alignment and photometric measurements. The image guide, which suffers severe transmission loss from exposure to ionizing radiation, is recalibrated after each day of plasma operations and replaced when its transmission falls to a few percent of its original value. Heating of the image guide to 150°C in an ex-situ vacuum furnace for 48 h was found to restore its transmission to >90% of its original value. Apart from the image guide, no significant degradation of the ex-vessel optical components has been observed over a period of four years or 10 hours of DIII-D plasma operations. The reflectivity of the in-vessel mirror, however, decreased by a factor of 2 to 3 over the course of two years of plasma operations due, most likely, to the formation of carbon films on the mirror surface.

Raw video data are acquired during plasma operation and stored on an MDSplus server. The 2-D emissivity distributions in the poloidal plane are calculated from the raw images using tomographic reconstruction techniques. Spatial resolution of 2 cm in the region of interest has been achieved in the reconstructed intensity distribution. These data are further processed to yield 1-D poloidal profiles along lines-of-sight of other optical diagnostics in DIII-D, e.g., the filterscope system. The camera data was found to be consistent with the filterscope brightness measurements to within a factor of 2 in the

same plasma discharge. The calibrated and processed camera data are stored in MDSplus format.

Highlights of measurements with the midplane camera system include measurements of the high-field and low-field SOL emission from deuterium neutrals and low charge-state carbon ions, during standard operation and during injection of methane for transport studies. Additionally, microsecond long snapshots of argon emission during massive gas jet injection have been obtained. These data are instrumental in validating edge plasma transport models for predictions of the SOL properties, such as heat flux and material erosion in future, fusion-relevant devices.

ACKNOWLEDGMENT

References

[1]   A. Loarte, B. Lipschultz, A. S. Kukushkin, G. F. Matthews, P. C. Stangeby, N. Asakura, G. F. Counsell, G. Federici, A. Kallenbach, K. Krieger, A. Mahdavi, V. Philipps, D. Reiter, J. Roth, J. Strachan, D. Whyte, R. Doerner, T. Eich, W. Fundamenski, A. Herrmann, M. Fenstermacher, P. Ghendrih, M. Groth, A. Kirschner, S. Konoshima, B. LaBombard, P. Lang, A. W. Leonard, P. Monier-Garbet, R. Neu, H. Pacher, B. Pegourie, R. A. Pitts, S. Takamura, J. Terry, E. Tsitrone and the ITPA Scrape-off Layer and Divertor Physics Topical Group, Nucl. Fusion **47**(6), S203 (2007).

[2]   B. Lipschultz, X. Bonnin, G. Counsell, A. Kallenbach, A. Kukushkin, K. Krieger, A. Leonard, A. Loarte, R. Neu, R. A. Pitts, T. Rognlien, J. Roth, C. Skinner, J. L. Terry, E. Tsitrone, D. Whyte, S. Zweben, N. Asakura, D. Coster, R. Doerner, R. Dux, G. Federici, M. Fenstermacher, W. Fundamenski, P. Ghendrih, A. Herrmann, J. Hu, S. Krasheninnikov, G. Kirnev, A. Kreter, V. Kurnaev, B. LaBombard, S. Lisgo, T. Nakano, N. Ohno, H. D. Pacher, J. Paley, Y. Pan, G. Pautasso, V. Philipps, V. Rohde, D. Rudakov, P. Stangeby, S. Takamura, T. Tanabe, Y. Yang and S. Zhu, Nucl. Fusion **47**, 1189 (2007) .

[3]   M. E. Fenstermacher, S. L. Allen, D. N. Hill, R. C. Isler, C. J. Lasnier, A. W. Leonard, T. W. Petrie, G. D. Porter, W. P. West, D. G. Whyte, R. D. Wood, Rev. Sci. Instrum. **68**, 348 (1997).

[4]   J. Gafert, K. Büchl, M. E. Fenstermacher, W. H. Meyer and the ASDEX Upgrade Team, *Reconstruction of the two-dimensional emissivity distributions in the ASDEX Upgrade LYRA-Divertor from TV-CCD-Data*, Proc. 26th EPS Conf. on Contr.

Fusion and Plasma Physics (Maastricht, The Netherlands, 1999), ECA Vol. 23J, p. 1577.

[5] K. Itami, P. Coad, W. Fundamenski, C. Ingesson, J. Lingertat, G. F. Matthews, A. Tabasso, J. Nucl. Mater. **290-293**, 633 (2001).

[6] C. J. Boswell, J. L. Terry, B. Lipschultz, J. Stillerman, Rev. Sci. Instrum. **72**, 935 (2001).

[7] A. Huber, P. Coad, D. Coster, L. C. Ingesson, K. Itami, S. Jachmich, A. Kirschner, M. Lehnen, G. F. Matthews, Ph. Mertens, V. Philipps, A. Pospieszczyk, B. Schweer, G. Sergienko, M. Stamp and Contributors to the EFDA-JET Programme, J. Nucl. Mater. **313-316**, 925 (2003).

[8] A. Patel, P. G. Carolan, N. J. Conway, C. A. Bunting, R. J. Akers, Rev. Sci. Instrum. **75**, 4145 (2004).

[9] A. L. Roquemore, Ted Biewer, D. Johnson, S. J. Zweben, Nobuhiro Nishino, V. A. Soukhanovskii, Rev. Sci. Instrum. **75**, 4190 (2004).

[10] J.L. Luxon, Nucl. Fusion **42**, 614 (2002).

[11] D. G. Nilson, M. E. Fenstermacher, R. Ellis, G. Brewis, N. Jalufka, R. T. Snider, Rev. Sci. Instrum. **70**, 738 (1999).

[12] SCHOTT North America, Inc., 555 Taxter Road, Elmsford, New York 10523 USA, http://www.us.schott.com

[13] M. Groth, M. E. Fenstermacher, C. J. Lasnier, R. Hernandez, J. M. Moeller, R. A. Sturz, Rev. Sci. Instrum. **74**, 2064 (2003).

[14] Persistence of Vision Raytracer Pty. Ltd., P.O. Box 407, Williamstown, Victoria 3016, Australia, http://www.povray.org/

[15]   Optronics Laboratories, 4632 36th Street Orlando, Florida 32811, http://www.olinet.com/

[16]   P.D. Morgan, *Irradiation of optical fibres at JET through 14 MeV neutron production*, Proc. 17th Symp. on Fusion Technology (Rome, Italy, 1992), edited by G. Ferro, M. Gasparotto, and H. Knoepfel (Elsevier, New York, 1992), Vol. 1, p. 722.

[17]   A. T. Ramsey and K. W. Hill, Rev. Sci. Instrum. **63**, 4735 (1992).

[18]   W. W. Heidbrink, P. L. Taylor, J. A. Phillips, Rev. Sci. Instrum. **68**, 536 (1997).

[19]   A.T. Ramsey, Rev. Sci. Instrum. **66**, 871 (1997).

[20]   P.L. Taylor, private communications.

[21]   J.F. Baur, B.A. Engholm, M.O. Hacker, I. Maya, P.H. Miller, W.E. Toffolo, S.S. Wojtowicz, *Radiation hardening of diagnostics for fusion reactors*, General Atomics Inc. Report GA-A16614 (1981).

[22]   SLATEC Common Mathematical Library, Version 4.1, July 1993, http://www.netlib.org/slatec/

[23]   The Numerical Algorithms Group, http://www.nag.co.uk/

[24]   Jason Cantarella, UGA Mathematics Department, Athens Georgia 30602, http://www.jasoncantarella.com

[25]   R. J. Colchin, D. L. Hillis, R. Maingi, C. C. Klepper, N. H. Brooks, Rev. Sci. Instrum. **74**, 2068 (2003).

[26]   M. Groth, L. W. Owen, G. D. Porter, N. H. Brooks, M. E. Fenstermacher, W. H. Meyer, A. W. Leonard, T. W. Petrie, D. L. Rudakov, G. Wang, J. G. Watkins, N. S. Wolf, J. Nucl. Mat. **337-339**, 425 (2005).

[27] E. M. Hollmann, T. C. Jernigan, M. Groth, D. G. Whyte, D. S. Gray, M. E. Austin,
B. D. Bray, D. P. Brennan, N. H. Brooks, T. E. Evans, D. A. Humphreys, C. J.
Lasnier, R. A. Moyer, A. G. McLean, P. B. Parks, V. Rozhansky, D. L. Rudakov,
E. J. Strait, W. P. West, Nucl. Fusion **45**, 1046 (2005).

TABLE 1. List of interference filters and measured plasma species in the DIII-D tokamak.

Filter wavelength/bandpass (nm/nm)	Plasma species/spectroscopic line
656.4/1.0	Deuterium/D_α
430.0/3.0	Hydrocarbon/CD
514.7/5.0	Carbon/CII
465.0/3.0	Carbon/CIII
580.3/1.0	Carbon/CIV
640.0/5.0	Neon/NeI
696.0/5.0	Argon/ArI
612.0/5.0	Argon/ArII

Figure captions

FIG. 1. (Color On-line) Midplane cross-section of the DIII-D vessel between 0 and 180° azimuth showing the tangential view fans of the LLNL midplane camera system superposed. The main view in the counter-clockwise direction has rays tangential to the SOL on the HFS, but not on the LFS. A tangential view of the SOL on the LFS in the clockwise direction was obtained by mounting a mirror on the shutter of an adjacent diagnostic system [beam emission spectroscopy (BES)].

FIG. 2. (Color On-line) Views through the tangential port using (a) a standard camera and (b) the image guide/CID camera assembly. Some vessel structures are called out.

FIG. 3. (Color On-line) Schematic layout of the optical system in the DIII-D tokamak hall.

FIG. 4. Schematic layout of the filter wheel and CID camera assembly. The micrometer stage (4) can be moved in the horizontal and vertical direction as indicated by the arrows.

FIG. 5. (Color On-line) (a) Image of the calibration board and (b) simulation of the field-of-view from POVRAY. A subset of the actual points on the calibration board is used to generate the virtual camera view.

FIG. 6. (Color On-line) Intensity calibration of the optical system for two wavelength filters: (a) D_α (656 nm) and (b) CIII (465 nm). The measured counts obtained between 2003 and 2007 are shown as a function of gain setting on the camera control unit.

FIG. 7. (Color On-line) Images of a calibration board before (a) and after (b) baking the image guide in vacuum at 150°C for 48 hours. The intensity difference is due to slightly different illumination of the calibration board. The loss of transmission due to ionizing radiation at a fluence of 6×10^{-15} n/m^2 (red curve and squares) and recovery of transmission by the bake (blue curve and diamonds) is shown in (c). The black curve and circles is the transmission of an unexposed image guide IG-154. The three vertical dashed lines mark the D_α, CII (515 nm), and CIII (465 nm) wavelengths used in this study.

FIG. 8. Transmission loss due to ionizing radiation in the Schott image guide IG-154 for three different wavelengths (red – D_α, green – CII 515 nm, blue – CIII 465 nm). The plot contains data from four different images guides (circles and triangles, both closed and open symbols). The neutron fluence is calculated from the measured neutron rate and an assumed distance of 3 m from the source to the guide. Application of linear regression analysis to the data yields slopes of 1.2×10^{-16}, 2.9×10^{-16}, and 4.1×10^{-16} at 656 nm, 515 nm, and 465 nm, respectively.

FIG. 9. (Color On-line) Intensity calibration of the LFS optical system at two wavelengths: (a) D_α (656 nm) and (b) CIII (465 nm). The black squares, red circles and blue triangles, respectively, correspond to view without mirror, view with in-vessel mirror prior to plasma exposure, and view with mirror after exposure to one year of plasma operations. The data are plotted as functions of the gain setting on the camera control unit, which is proportional to the voltage applied at the intensifier microchannel plate.

FIG. 10. (Color On-line) Photographs of mirror before (a) and after (b) plasma operations in 2006. Some reflections off the vacuum vessel are seen as darkened areas. An oblique black stripe visible after plasma operations in indicated by the red arrow.

FIG. 11. Measurement of the 3-D profile of CIII emission in DIII-D discharge 119919 at 3 s (a). The camera field-of-view is indicated by the white trapezoid. The 3-D data is tomographically reconstructed into the 2-D poloidal plane (b), and further processed into a 1-D poloidal profile (c). In (b) the viewing geometry of the multi-channel virtual filterscope system is indicated by the gray triangle, and the actual viewing geometry of the radial midplane filterscope is shown in red. The measured line-integrated CIII emission from the actual filterscope is plotted in (c) along with the calculated brightnesses from the camera as function of height along the HFS wall.

FIG. 12. (Color On-line) 3-D profiles of CIII emission prior to (a) and during methane injection (b) in DIII-D discharge 129896 (3 s and 4 s, respectively). The main and mirror fields-of-view are indicated by the white dashed trapezoids. The emission from the HFS SOL region was attenuated by a neutral density filter of OD = 1.0. Figures (c) and (d) show profiles of the CIII emission in the HFS and LFS SOL, respectively, along the radial paths between the white crosses indicated in (a).

FIG. 13. (Color On-line) Snapshot of duration 20 μs for ArII emission during massive gas injection (DIII-D discharge 117473 at 3.037 s). Vessel features in the upward-canted viewing geometry are indicated with white dashed lines.
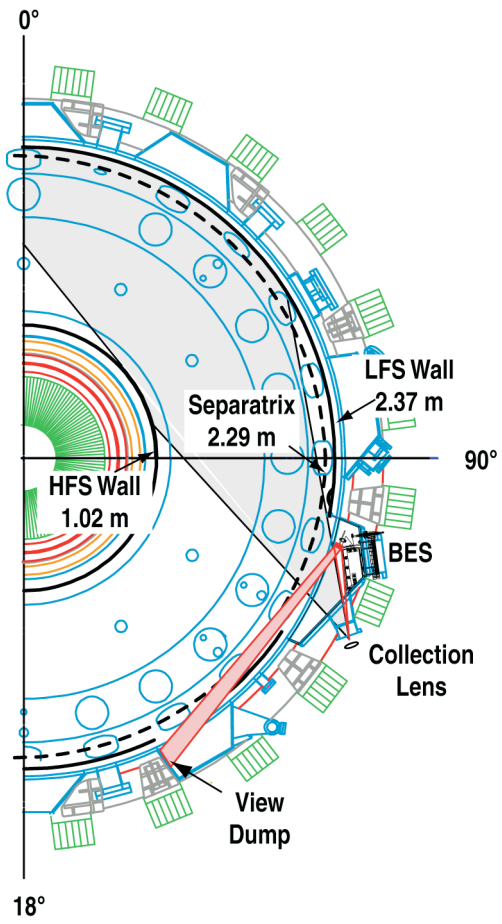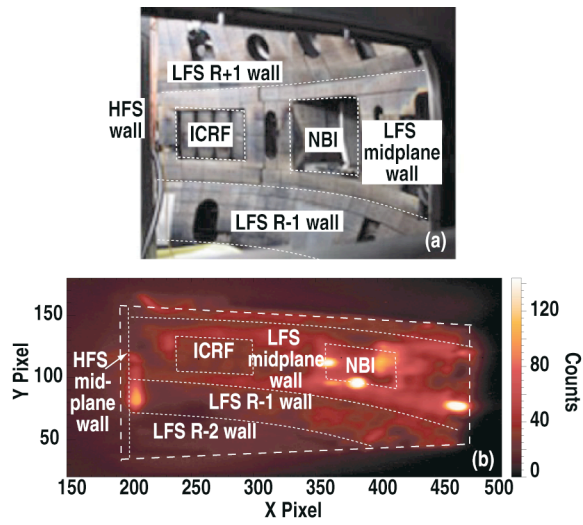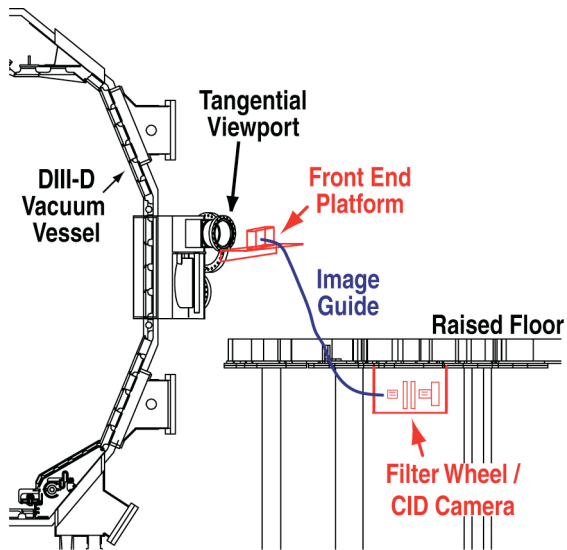
Fig. 1, M. Groth, RSI
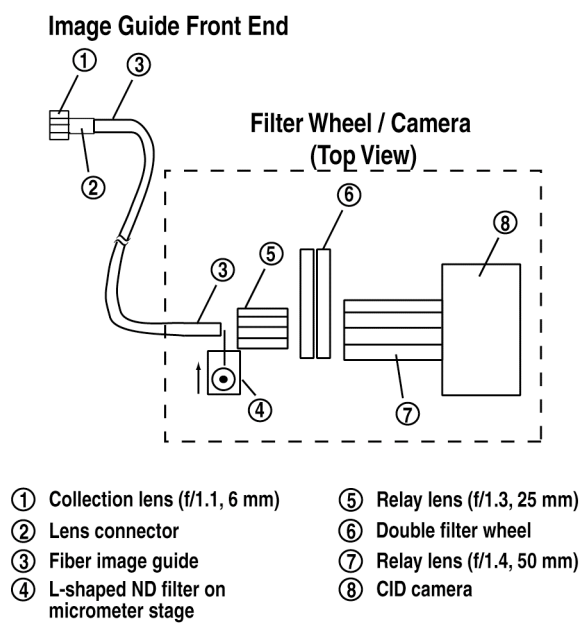
Fig. 2, M. Groth, RSI

Fig. 3, M. Groth, RSI

Image Guide Front End

Filter Wheel / Camera (Top View)

① Collection lens (f/1.1, 6 mm) ⑤ Relay lens (f/1.3, 25 mm)
② Lens connector ⑥ Double filter wheel
③ Fiber image guide ⑦ Relay lens (f/1.4, 50 mm)
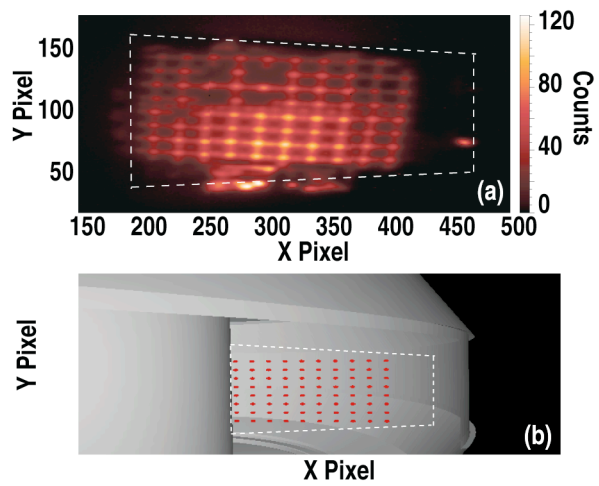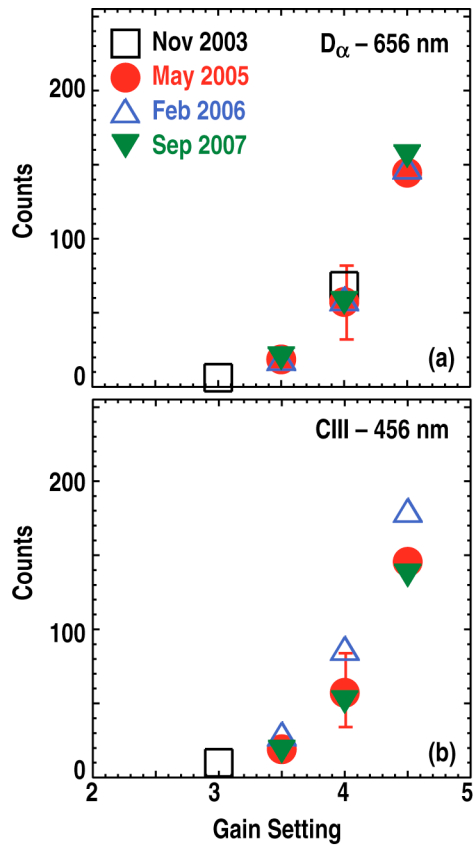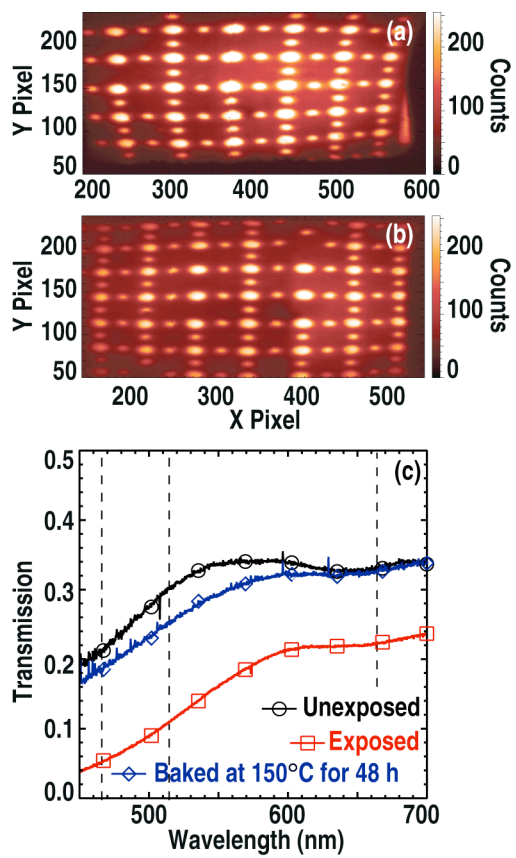④ L-shaped ND filter on micrometer stage ⑧ CID camera

Fig. 4, M. Groth, RSI

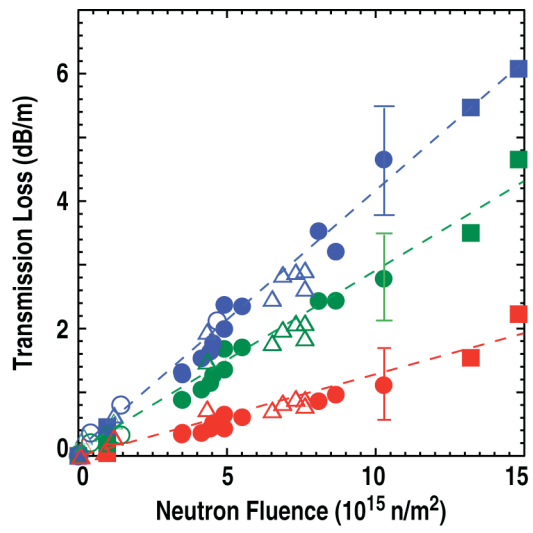Fig. 5, M. Groth, RSI

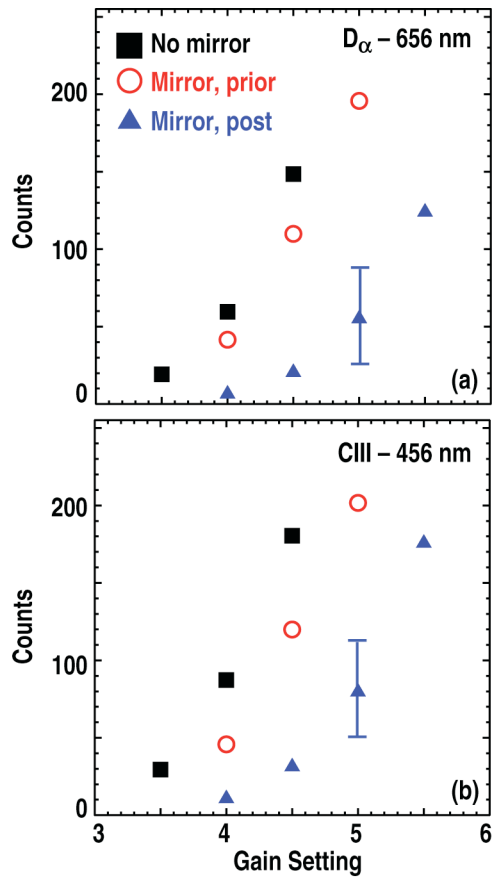Fig. 6, M. Groth, RSI

Fig. 7, M. Groth, RSI

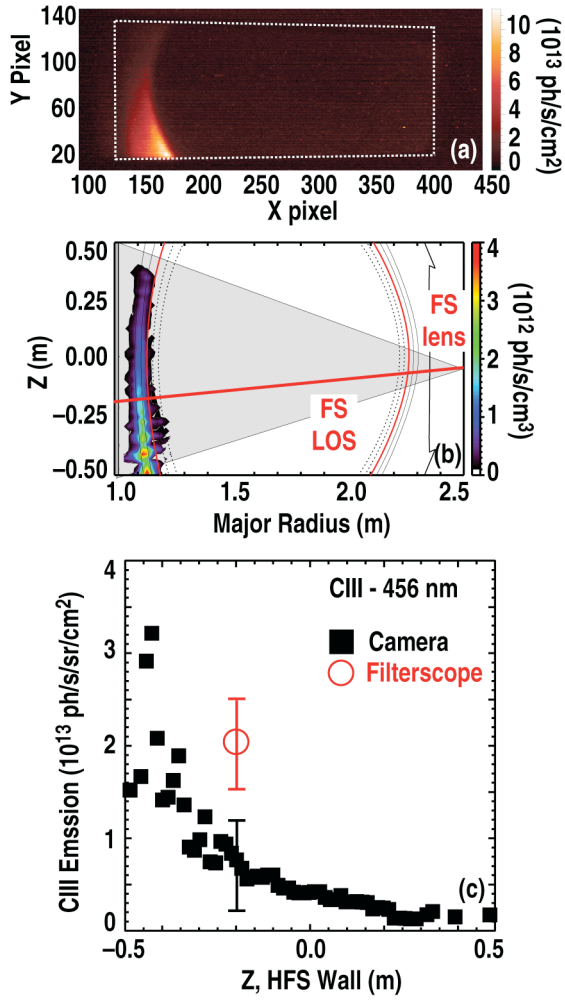Fig. 8, M. Groth, RSI
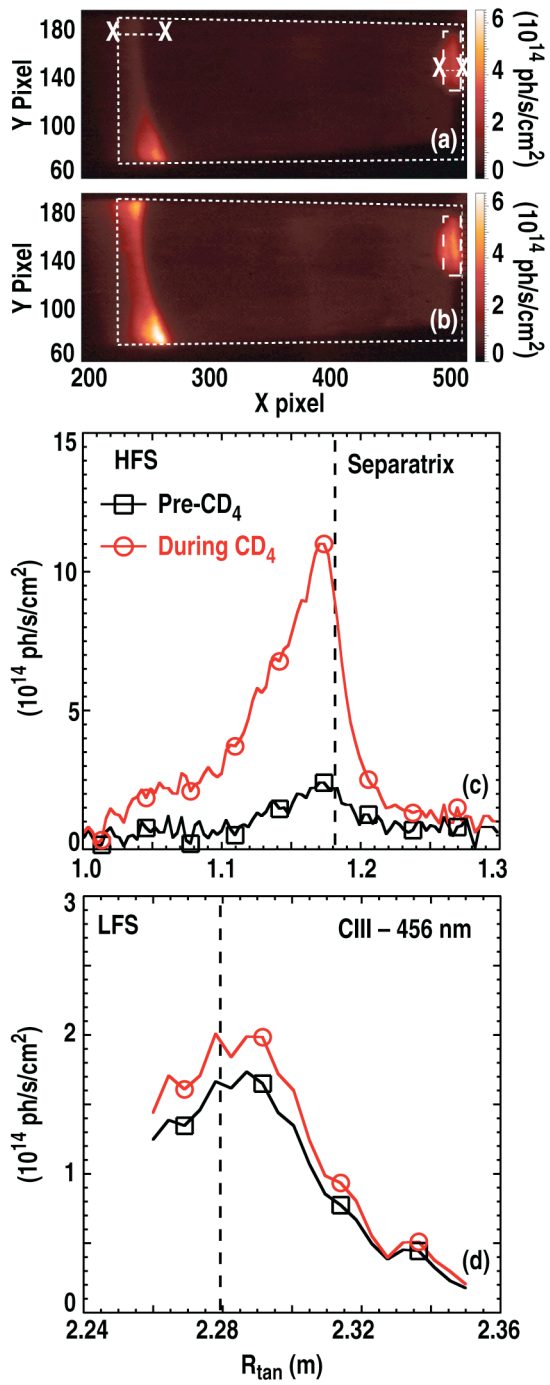
Fig. 9, M. Groth, RSI

Fig. 10, M. Groth, RSI
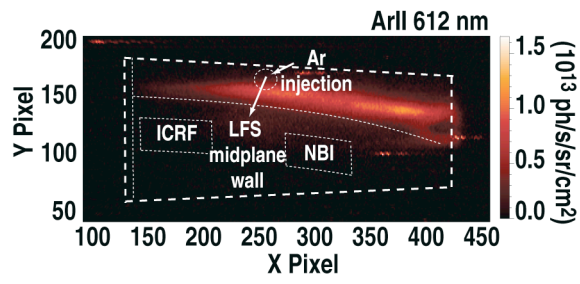
Fig. 11, M. Groth, RSI

Fig. 12, M. Groth, RSI

Fig. 13, M. Groth, RSI